HHS Public Access

Author manuscript

J Nanotoxicol Nanomed. Author manuscript; available in PMC 2018 January 10.

Published in final edited form as:

J Nanotoxicol Nanomed. 2017 ; 2(1): 11–27. doi:10.4018/JNN.2017010102.

Assessment of Crystal Morphology on Uptake, Particle Dissolution, and Toxicity of Nanoscale Titanium Dioxide on *Artemia salina*

Martha Johnson,
Department of Chemistry and Biochemistry, Jackson State University, Jackson, MS 39217 USA

Mehmet Ates,
Department of Bioengineering, Munzur University, Faculty of Engineering, Tunceli, 62000, Turkey

Zikri Arslan,
Department of Chemistry and Biochemistry, Jackson State University, Jackson, MS 39217 USA

Ibrahim Farah, and
Department of Biology, Jackson State University, Jackson, MS 39217

Coneliu Bogatu
Institute of Industrial Ecology, Timisoara, Romania

Abstract

Knowledge of nanomaterial toxicity is critical to avoid adverse effects on human and environment health. In this study, the influences of crystal morphology on physico-chemical and toxic properties of nanoscale TiO_2 (*n*-TiO_2) were investigated. *Artemia salina* were exposed to anatase, rutile and mixture polymorphs of *n*-TiO_2 in seawater. Short-term (24 h) and long-term (96 h) exposures were conducted in 1, 10 and 100 mg/L suspensions of *n*-TiO_2 in the presence and absence of food. Anatase form had highest accumulation followed by mixture and rutile. Presence of food greatly reduced accumulation. *n*-TiO_2 dissolution was not significant in seawater ($p<0.05$) nor was influenced from crystal structure. Highest toxic effects occurred in 96h exposure in the order of anatase > mixture > rutile. Mortality and oxidative stress levels increased with increasing *n*-TiO_2 concentration and exposure time ($p<0.05$). Presence of food in the exposure medium alleviated the oxidative stress, indicating that deprivation from food could promote toxic effects of *n*-TiO_2 under long-term exposure.

Keywords

Nanoscale titanium oxide; Crystal morphology; Anatase; Rutile; Accumulation; Particle dissolution; Toxicity; *Artemia salina*

INTRODUCTION

Our understanding about the environmental and human health effects of nanoscale materials is still in its infancy despite growing research exploring the environmental and biological fate and toxicity of nanomaterials (Scown, van Aerle & Tyler, 2010). This is mainly because the physico-chemical and toxicological properties of materials at nanoscale are a complex

phenomenon governed by numerous parameters. Nanomaterials possess very large surfaces (e.g., more atoms per unit area) owing to their extremely small size (1–100 nm), which evidently results in larger contact surfaces and liberation of more toxic elements and ions upon degradation, respectively. Particle size, shape/morphology, surface charge and methods of synthesis also impart significant differences in toxicological properties of nanomaterials (Hu et. al, 2009; Huang, Wu & Aronstam, 2010). Moreover, the physiochemical conditions of test environment (e.g., salinity, pH, temperature, light etc.) and the resilience of model organism may alter observed effects.

Titanium dioxide nanoparticles (*n*-TiO_2) exhibit photocatalytic and antibacterial properties under UV-light (Lai et al., 2008). In recent years, *n*-TiO_2 have been extensively used in various consumer products, including sunscreens, toothpaste, food additives, paints, surface coatings, water disinfection and degradation of pollutants in air and soil (Nowack & Bucheli, 2007; Battin et al., 2009; Weir et al., 2012; Jovanovi, 2015). *n*-TiO_2 is considered an aquatic pollutant due to numerous exterior uses and applications in water treatment. Nevertheless, the information about safety of *n*-TiO_2 to aquatic environments and species is controversial though it is among the earliest nanoscale compounds investigated extensively so far (Jovanovi, 2015). Some groups did not observe any adverse effects on different biological species (Lovern & Klaper, 2006; Lai et al., 2008; Aruoja et al., 2009, Zhu et al., 2011, Fang et al., 2015), while some others reported dose dependent toxic effects (Heinlaan et al., 2008; Zhu et al., 2010; Ates et al., 2013a; Mansfield et al., 2015). For instance, *n*-TiO_2 was reported to be more toxic to microalgae *Pseudokirchneriella subcapitata* (LC_{50} = 5.83 mg L^{-1}) than bulk TiO_2 (LC_{50} = 35.9 mg L^{-1}) (Aruoja et al., 2009). In contrast, no apparent toxicity was observed from *n*-TiO_2 to crustaceans *Daphnia magna* and *Thamnocephalus paltyurus*, and the bacteria *Vibrio fischeri* (Heinlaan et al., 2008), but previously exposed *Daphnia magna* offsprings were found more sensitive to *n*-TiO_2 (Bundschuh et al., 2012). Similarly, aqueous suspensions of *n*-TiO_2 were not acutely toxic but induced oxidative stress on marine abalone (*Haliotis diversicolor supertexta*) (Zhu et al., 2011). Japanese medaka (*Oryzias latipes*) embryos showed premature hatching and high mortality from chronic exposure to *n*-TiO_2 (Paterson et al., 2011). Toxicity to rainbow trout (*Oncorhynchus mykiss*) varied with the route of exposure (Handy et al., 2008). Direct exposure to *n*-TiO_2 colloids caused severe adverse effects whereas no acute toxicity was detected from dietary exposure.

Titanium dioxide (TiO_2) is found in nature in three major polymorphs; anatase, rutile and brookite that exhibit varying degrees of photo-catalytic properties (Liu et al., 2012). Rutile and anatase are most abundant. Of these, rutile is also known as the most stable and benign crystalline form of TiO_2. Anatase is a less dense, softer form of TiO_2 that possess higher catalytic activity owing relatively larger band gap energy (about 3.0 eV for rutile and 3.2 eV for anatase) which imparts more oxidation power and deeper surface activity of the electrons of anatase than rutile (Liu et al., 2012; Luttrell et al., 2014). The literature regarding the toxicological effects of *n*-TiO_2 clearly show that observed effects vary substantially with concentration, species or test models, and duration of exposure. In addition, in most studies the *n*-TiO_2 utilized was either purely anatase (Paterson et al., 2011; Mansfield et. al., 2015), purely rutile (Ates et al., 2013a), or a mixture of rutile and anatase (Zhu et al., 2010; Kim et al., 2010). It is, however, difficult to pinpoint the influence of crystal morphology (e.g., crystal phase) on the overall toxicity of *n*-TiO_2 among totally different test environments and

organisms/species. Anatase form was found more toxic than anatase/rutile mixture to human lung epithelial cells (Hsiao & Huang, 2011). DeMatteis et al. (2016) also reported that anatase polymorph could be more prone to degradation and physicochemical stresses (pH, light exposure) to cause higher toxic effects. Therefore, there is a need to investigate different crystal polymorphs *n*-TiO_2 systematically and simultaneously to elucidate their physicochemical and toxicological properties.

In this study, we performed exposures on brine shrimp (*Artemia salina*) with anatase, rutile polymorphs of *n*-TiO_2 and their mixture (anatase/anatase) in an attempt to determine the influences of crystal polymorph on particle uptake, degradation (ion release), agglomeration, and toxicity. In an acute exposure, *Artemia salina* larvae were exposed to 1, 10 and 100 mg/L aqueous suspensions of anatase, rutile, and the anatase/rutile mixture of *n*-TiO_2 in seawater for 24 and 96 h under 16 h light and 8 h dark regime. Accumulation (e.g., total body burden) and free Ti ion levels were determined by inductively coupled plasma mass spectrometry (ICP-MS) analyses of exposed artemia and exposure medium (seawater) samples, respectively. Toxic effects were examined by determining mortality and malondialdehyde (MDA) levels as a lipid peroxidation biomarker in tissues of exposed artemia.

MATERIALS AND METHODS

Titanium dioxide nanoparticle and preparation of suspensions

Uncoated *n*-TiO_2 powders of anatase (10–30 nm, 99.5%) and rutile (10–30 nm, 99.5%) polymorphs and mixture of anatase/rutile (10–30 nm, 30% rutile and 70% anatase) were purchased from Skyspring Nanomaterials Inc., Houston, TX USA. Some physical properties of these nanopowders are summarized in Table 1. Aqueous suspensions were prepared as described elsewhere (Ates et al., 2013a). Briefly, 1% (m/v) *n*-TiO_2 (e.g., 10,000 mg/mL) stocks were prepared by dispersing appropriate amount of each *n*-TiO_2 powder in 100 mL deionized water. These suspensions were vortexed for 20 s, and then sonicated in an ultrasonic bath for about 10 min for maximum dispersion. Then, appropriate volumes were immediately transferred into the exposure tanks containing *Artemia salina* larvae in seawater.

Artemia cysts (The Great Salt Lake, Utah harvest) were purchased from Artemia International LLC, Houston TX, and were kept in a refrigerator at 4°C. High purity acids were used for instrumental chemical analyses. Hydrofluoric acid (HF, 99.999%) was purchased from Sigma Aldrich. Trace metal grade nitric acid (HNO_3) was procured from Fisher Scientific. Carbon coated Cu TEM grids (300 mesh) were purchased for Electron Microscopy Sciences (EMS), Hatfield, PA and used in measurement of particle size of *n*-TiO_2 in stocks and experimental colloids.

Characterization of *n*-TiO_2 powders

The characterizations of *n*-TiO_2 powders were performed by using X-ray diffraction (XRD), Fourier transform infrared spectroscopy (FT-IR), scanning electron microscopy (SEM) and transmission electron microscopy (TEM), and dynamic light scattering (DLS). XRD

measurements were carried out using a Rigaku Ultima IV X-ray powder diffractometer with CuKα radiation (λ=0.54056 nm). FT-IR spectra of the *n*-TiO_2 powders were recorded from their KBr pellets using a JASCO FT/IR-4100 spectrometer in the range of 400–4000 cm^{-1}. Spectra were collected in single beam mode with 16 scans at 4 cm^{-1} resolution. The surface morphology of *n*-TiO_2 was studied by scanning electron microscopy (SEM) with the instrument KYKY-EM3200.

TEM measurements were made with JEOL-1011 TEM instrument with 0.2 nm lattice resolution and magnification power up to 10^6 under the accelerating voltage of 40 to 100 kV. For TEM measurements, 10 μL of aqueous suspension were dropped on a carbon-coated copper grid (CF300 Cu) and allowed to dry overnight. Captured images were analyzed using ImageJ software. Hydrodynamic size of experimental colloids and zeta-potentials were measured with a Nano ZS Zetasizer (Malvern Instruments). For zeta potential measurements, 10 μg/mL colloidal solutions of *n*-TiO_2 powders were prepared in deionized water. A portion of the suspension was vortexed and placed into zeta cell (Malvern Instruments, DTS1060C) and measured at 25 °C. DLS measurements were made from same 10 μg/mL colloidal solutions. Three DLS measurements were taken successively for each solution to estimate hydrodynamic particle size distribution in water.

Test organism preparation

Artemia salina cysts (The Great Salt Lake, UT) were hatched in seawater (3% wt). The seawater was prepared by dissolving Instant Ocean® salt (Aquatic Eco–Systems, Apopka, FL) in deionized water and stirred for 24 h under aeration and then filtered through 30–μm Millipore cellulose filters before use. Cysts were hatched as described in previous publications (Ates et al. 2013a, 2013b). Encysted artemia were first hydrated in distilled water at 4 °C for 12 h. The floating cysts were removed by successive wash with water. The sinking cysts were collected on a Buchner funnel and washed with cold deionized water followed by the rested seawater. Approximately 3 g of cleaned *Artemia* cyst were incubated in 1.5 L of seawater (pH 8.3–8-5) at 30 ± 2 °C under a 1500 lux day-light. Air was pumped through the bottom of the container to prevent settling of cysts. Hatching completed within 24 to 36 h.

The number of artemia larvae in the stock was counted before exposure to deliver comparable number of artemia for each tank. Briefly, 100 mL seawater containing hatched artemia was taken into a pre-cleaned beaker. Under continuous stirring, 1.0 mL of this stock was transferred to another 100 mL seawater (100–fold dilution). A volume of 0.1 mL was taken under stirring and placed in a petri–dish, and *Artemia salina* were visually counted.

Exposure of *Artemia salina* larvae to *n*-TiO_2 suspensions

Artemia salina cultures were exposed to 1, 10 and 100 mg/L aqueous colloidal solutions of anatase, rutile, and anatase/rutile polymorphs of *n*-TiO_2. Acute exposure was conducted for a period of 24 and 96 h for each polymorph according to Organization for Economic Cooperation and Development, OECD 202 testing guidelines (OECD 2004). The exposure regimes are summarized in Table 2. A control group was also setup without the test compound. Studies were carried out in 500 mL seawater in conical containers with

graduations (1.0 L inner volume). Aeration was provided by a line extending to the bottom of the conical flask. Each scheme (controls or treatments) was conducted in triplicate in the presence and absence of food (see Table 2). Planktonic algae commercially purchased were diluted and given to artemia as food. At the beginning, a volume of 5 mL of algae was delivered to all controls and treatments designated as “exposure with food”. No food was provided to those designated as “exposure without food”. Light regime of 16:8 h light: dark and temperature of 24 ± 2 °C were maintained. During the exposure, the salinity and pH of the seawater were monitored for assurance of conditions to artemia. At the end of the exposure, artemia were immediately washed and filtered for further analysis.

Determination of *n*-TiO_2 accumulation and particle dissolution

Determination of *n*-TiO_2 accumulation in artemia was carried out by ICP-MS analysis using a Varian 820MS ICP-MS instrument (Varian, Australia). Exposed artemia were sampled after 24 h and 96 h and thoroughly washed with deionized water through 5 μm plankton net. The cleaned samples were then filtered by 0.47 μm (pore diameter) Whatman filter paper. About 0.2 g of wet *A. salina* were weighed and digested in Teflon vessels in 2 mL HNO_3 and 0.5 mL HF at 160 °C for 2 h on a digestion block (DigiPrep MS, SCP Science). HF was required for total dissolution *n*-TiO_2. All digests were first diluted to 10 mL with water. A 10-fold dilution was made for ICP-MS analysis. For quality control, pure *n*-TiO_2 powders (ca. 10 mg, n=3) were digested in 3 mL HNO_3 and 1.0 mL HF and diluted to 10 mL with water. These samples were diluted 1000-fold before analysis (Ates et al., 2013a).

To determine the extent of particle dissolution for anatase, rutile, and anatase/rutile mixture, 5 mL of respective suspensions were taken up 24 h and 96 h later from the exposure containers. The suspensions were first centrifuged for 30 min at 10,000 rpm to remove large particles. In the next step, 0.5 mL of supernatant was taken and passed through 3 kDa ultrafiltration cartridges (1.2 nm pore size, VWR International) to separate dissolved Ti ions from suspending nanoparticles. The supernatant solution from the ultrafiltration was diluted to 1 mL with 10% HNO_3 and analyzed by ICP-MS for dissolved Ti in medium. Titanium standard solutions ranging from 0.1 to 100 μg/mL Ti were used for calibration of ICP-MS instrument. Data were collected with ^{47}Ti and ^{49}Ti isotopes. Titanium levels measured from the digested artemia samples were converted to determine equivalent mass of TiO_2 taken up by artemia larvae.

Assessment of mortality and oxidative stress

At the conclusion of the exposures, mortality rates were determined to verify potential toxicity of anatase, rutile, and anatase/rutile mixture of *n*-TiO_2 suspensions. The exposed artemia larvae were counted from their suspensions as described above for the stocks artemia culture (Ates et al., 2013a). Dead artemia were realized as immobile species that were unable to swim and consequently settled rapidly during counting in Petri-dish.

The extent of oxidative stress caused by the *n*-TiO_2 suspensions were measured with malondialdehyde (MDA) assay using thiobarbituric acid reactive substances (TBARS) method. MDA is a low molecular weight, colorless by–product of lipid peroxidation, which reacts with thiobarbituric acid to yield a colored complex that absorbs strongly at 530–535

nm. . The MDA levels were measured as described elsewhere (Van et al 1990; Ates et al., 2013a, 2013b). Samples were assayed immediately after the exposure. About 0.2 g *Artemia salina* were washed with cold water and then assayed using MDA assay kit (Northwest Life Science, LLC, Vancouver, WA). Samples were homogenized in 2 mL phosphate buffer solution (pH 7.2) by a Fisher Scientific Model 100 Sonic Dismembrator equipped with titanium probe and then centrifuged at 6,000 rpm for 10 min. The resulting supernatant was used for biochemical assay immediately. Briefly, 10 μL butylated hydroxytoluene (BHT), 0.25 mL of sample supernatant, 0.25 mL of phosphoric acid (1.0 M), and 0.25 mL of TBA were added to a vial. A set of MDA standards were freshly prepared from tetramethoxypropane in a concentration range of 0 to 10 μM. All samples and standards were incubated at 90 °C for 1 h, and then centrifuged at 12,000 rpm for 15 min to separate suspending tissues. The absorbance of the supernatant was measured at 532 nm by a spectrophotometer. Measurements were performed in triplicate for all experimental groups. The values of TBASR were expressed as total MDA per gram of *Artemia*.

Statistical analysis

The data were recorded as the mean and standard deviation. One-way analysis of variance (ANOVA) with Turkey's multiple comparisons was used to detect significant differences in accumulation, particle degradation/dissolution, mortality, and toxicity. A p-value of < 0.05 was considered statistically significant.

RESULTS AND DISCUSSION

Powder XRD analysis of *n*-TiO_2 powders

The XRD patterns (2θ value) for anatase (10–25 nm), rutile (10–30 nm) and anatase/rutile mixture (10–30 nm) of *n*-TiO_2 are illustrated in Figure 1. The size of crystals were computed with Scherrer's equation; $d=0.89\lambda/\beta\cos\theta$, where d is the crystal size, θ is the diffraction angle, β is the full width at half maximum height, λ the wavelength of the X-ray (0.15406 nm) (Vijayalakshmi & Rajendran, 2012; Kadam et al., 2014). For anatase, the maxima of the diffraction peaks were recorded at 25.25°, 37.89°, 48.02°, 54.1°, 55.11°, 62.83°, 69.36°, 70.49°, and 75.31°. These values match with those of the card no. 21–1272 for nanocrystalline anatase from the data base of the Joint Committee on Powder Diffraction Standards (JCPDS) and those previously reported for pure anatase (Shirke et al., 2011; Kadam et al., 2014). The average crystallite size was computed to be 17.7 nm using the main peaks at 25.25° and 48.03°.

The XRD spectrum of rutile showed three main peaks with maxima at 27.39°, 36.10°, 54.28° and a series of smaller peaks at 39.14°, 41.16°, 44.11°, 56.52°, 62.85°, 64.15°, 69.10°, 69.94° that are consistent with reported values (Hussain & Wahab, 2014; El-Sherbiny et al., 2014). The positions of these peaks fit well with those from the card file no. 75–1753 of the data base of the JCPDS, which confirm purity of rutile TiO_2 (El-Sherbiny et al., 2014). Intense, sharp peaks are indicative of high crystallinity of rutile form. The average size of crystallites calculated from the main peaks was 21.3 nm. The XRD pattern of anatase/rutile mixture (Fig. 1) possessed diffraction peaks of anatase at the 2θ values of 25.37°, 38.02°, 47.95°, 54.8°, 62.71°, 69.83°, 75.19° and of rutile at 27.39°. The most

intense peak at 25.37° verifies that anatase form is compositionally predominant in the mixture. The average particle size of crystallite of the mixture was computed as 19.8 nm.

FT-IR spectra of *n*-TiO_2 powders

FTIR spectra of *n*-TiO_2 polymorphs are shown in Figure 2. The peaks and bands assigned are for anatase, rutile and the anatase/rutile mixture agree with the reported data. The band with maximum at 3432.7 cm^{-1} in FT-IR spectrum of anatase is assigned to OH stretching vibration from traces of water adsorbed on the oxide surface. Small peaks at 2928, 2852 cm^{-1} are due to stretching vibration of C-H bonds with very low of transmittances. The peak at 1627.7 cm^{-1} and a the shoulder at 1598 cm^{-1} are ascribed to OH bending vibration of water and to asymmetric stretching vibration of carboxylate COO^- group, respectively (Nolan, Pillai & Seery, 2009). The peaks from 1384.7 and 1354 cm^{-1} correspond to symmetric vibration of carboxylate and that at 1115 cm^{-1} (not indicated) to C-O bonds. There is a broad and intense band between 900 and 400 cm^{-1} with maximum at 526.5 cm^{-1}. This peak is assigned to Ti-O and Ti-O-Ti stretching and bending vibrations. This band has high value of transmittance and is characteristic to pure anatase polymorph of TiO_2 (El-Sherbiny et al., 2014).

FT-IR spectrum of rutile form of *n*-TiO_2 is similar to that of anatase. It contains a band with maximum at 3434.7 cm^{-1} due to OH stretching of water. The small peaks at 2924 and 2852 cm^{-1} are associated with C-H bonds. The peaks from 1384.7 and 1350 cm^{-1} are assigned to symmetric vibration of carboxylate (Nolan, Pillai & Seery, 2009). The intense band in the range of 830–400 cm^{-1} with maximum at 680.7 cm^{-1} and a shoulder at 536 cm^{-1} are specific to Ti-O vibration of pure rutile with high value of transmittance (El-Sherbiny et al., 2014; Kadam et al., 2014). The. FTIR spectrum of the anatase/rutile mixture shows the same bands and peaks as in the individual oxides. The maximum of the main band due to Ti-O bonds and Ti-O-Ti network ranged between those of anatase and rutile at 576.6 cm^{-1}.

Surface characterization of *n*-TiO_2 powders

The SEM images of the *n*-TiO_2 are shown in Figure 3. The anatase form (Fig. 3A) shows irregular morphology consisting of agglomerations with different sizes (Shirke et al., 2011). Spherical and long agglomerates ranging from 100 to 250 nm and as large as 1000 nm agglomerates were noted (Klein et al., 2003). It was reported that a small anatase agglomerate may consists of 3 to 5 crystallites, which are also consistent with the X-ray diffraction results for anatase (Vijayalakshmi & Rajendran, 2012). SEM images of rutile exhibit similar agglomerations as anatase. Anatase/rutile mixture also reveals small and large nanoparticle agglomerations in the range of 300–875 nm.

Particle size distribution of aqueous *n*-TiO_2 colloids

The TEM images recorded from *n*-TiO_2 colloids in deionized water and seawater are illustrated in Fig. 4. *n*-TiO_2 powders are highly hydrophobic, and thus agglomerate substantially in water (Ates et al., 2013a; Zhu et al., 2010). In this study, rutile showed lesser agglomeration in deionized water than both anatase and anatase/rutile mixture. In seawater, the particle size increased drastically and indistinguishable for all *n*-TiO_2 polymorphs. Similar effects have been reported previously and are due to the reduction of repulsive

surface charges by the ionic species in seawater. Besides agglomeration, size distribution was much larger in seawater colloids ranging from around 100 nm to as high as 1 μm for anatase, rutile and the anatase/rutile mixture.

Hydrodynamic sizes were recorded only for colloidal solutions (10 μg/mL) in deionized water since TEM data for the seawater suspensions had already shown substantial agglomeration. The results are summarized in Table 3 along with respective zeta potentials. Hydrodynamic sizes increased in the order of rutile < mixture ≤ anatase. As expected, hydrodynamic sizes of all *n*-TiO_2 polymorphs were higher than those recorded in their dried colloidal solutions as shown in Fig. 4A–C. Despite large size range (61–1152 nm), rutile *n*-TiO_2 showed smaller hydrodynamic size (432 nm) than both anatase (637 nm) and anatase/rutile mixture (662 nm). These results are consistent with those from SEM and TEM, indicating that rutile crystallites of *n*-TiO_2 were more stable in water against agglomeration. The zeta values also support this result. The surfaces of rutile *n*-TiO_2 possessed significantly higher negative charges (−31.6 ± 4.5 mV) to prevent agglomeration resulting from the reduction of electrostatic repulsion (surface charge) in water (Zhu et al., 2010; Zhu et al. 2011; Ates et al., 2013a). In contrast, the surface charge on anatase crystals and anatase/rutile mixture was not sufficiently high to prevent particle agglomeration. Consequently, both forms yielded relatively larger hydrodynamic sizes (see Z-average).

Effect of crystalline structure on dissolution of *n*-TiO_2 in seawater

Particle dissolution is considered a major pathway for release of free ions from metal and metal oxide nanoparticles to aquatic environments. Most nanotoxicity studies have reported dose-dependent toxic effects for metal and metal oxide nanoparticles, and consequently the observed toxic effects were partially attributed to the increased free metal concentration in the medium (Ates et al., 2013b; Jovanovi, 2015; DeMatteis et al., 2016). For instance, titanium ion concentration was higher for the suspensions of anatase polymorph in acidic pHs (DeMatteis et al., 2016). UV-light irradiation also reported to deteriorate the stability of anatase polymorph. In contrast, in this study, dissolved titanium levels for anatase, rutile and anatase/rutile mixture were not significant in seawater regardless of their crystalline phase (see Table 4). Nonetheless, time- and dose-dependent dissolution was noted. Specifically, dissolved titanium concentration increased significantly was from 24h to 96h. Interestingly, dissolution was more pronounced in dilute *n*-TiO_2 suspensions. In 96 h, for instance, dissolved Ti levels in 1 μg/mL colloidal solutions were 82.7, 86.4, and 84.6 ng/mL for anatase, rutile and anatase/rutile mixture. This accounts for about 12–13% dissolution. On the other hand, dissolved titanium levels were about 1.5 and 0.16% of the total titanium in the exposure medium (e.g., *n*-TiO_2) for 10 and 100 μg/mL *n*-TiO_2 colloids, respectively. It should be noted that particle agglomeration was also significant at elevated *n*-TiO_2 levels leading to formation of micron (μm) size massive aggregates. It appears that agglomeration led to reduced particle dissolution as the nanoparticles within the aggregates were more isolated and protected from surrounding seawater.

Effects of crystal phase and food availability on accumulation of *n*-TiO_2

Artemia are filter–feeders that ingest particles smaller than 50 μm (Ates et al., 2013a, 2013b). Despite substantial agglomeration, the hydrodynamic sizes of the TiO_2

agglomerates were still much smaller to ingest; consequently accumulation occurred rapidly (Figure 5). Total body burden of TiO_2 increased with nanoparticle concentration and exposure time for all *n*-TiO_2 polymorphs ($p < 0.05$). In 24-h exposure, for instance, average TiO_2 uptake in artemia exposed to 1 μg/mL anatase was 181 μg/g that increased to 833 μg/g and 1165 μg/g for 10 and 100 μg/mL suspensions. In 24-h exposure, accumulation was not affected from the differences in crystal phases of *n*-TiO_2 ($p < 0.05$); artemia accumulated the highest levels from the 100 μg/mL suspensions to similar levels indistinguishably (Fig. 5). Similar uptake patterns were observed in the presence of food, but the extent of TiO_2 accumulation was significantly lower ($p < 0.05$). Total TiO_2 accumulation in 24 h were about 185, 455 and 924 μg/g for 1, 10 and 100 μg/mL anatase suspensions, respectively. In previous studies, it was shown that elimination of ingested aggregates from the guts is very slow (Zhu et al 2010, Ates et al., 2013b). It was suggested that food particles facilitate the elimination process by preventing agglomeration of particles in the guts of artemia.

Prolonged exposure (96 h) resulted in elevated accumulation in a dose-dependent manner. Average TiO_2 accumulation from exposure to anatase form was 244, 1119 and 2338 μg/g for 1, 10 and 100 μg/mL suspensions. Those for rutile and anatase/rutile mixture were 161, 548, 1722 μg/g, and 189, 657, 2156 μg/g, respectively. Uptake levels were lower in the presence of food; 247, 1092 and 1592 μg/g for anatase, 123, 421, and 859 μg/g for rutile and 157, 538, and 1231 μg/g for the mixture from 1, 10 and 100 μg/mL suspensions, respectively. Unlike that in 24-h exposure, accumulation of rutile polymorph was significantly lower in 96 h than that of anatase and the mixture, especially for 100 μg/mL suspensions ($p < 0.05$). A similar pattern was noted for exposures in the presence of food indicating an accumulation order of rutile < mixture < anatase. Rutile phase was found to be the most stable crystal form in water possessing smaller aggregates. This could suggest that ingested rutile crystals could have been eliminated from the guts more effectively eliminated than larger aggregates of anatase and mixture.

Effects of *n*-TiO_2 crystal phase and food availability on *Artemia salina* mortality

The percent mortality rates resulting from exposure to anatase, rutile and anatase/rutile mixture suspensions shown in Fig. 6. Controls exhibited about 1.2% and 3.8% mortality within 24 h and 96 h, respectively ($p > 0.05$). This result indicated that presence or absence of food had no significant effect on the mortality rates in the absence of *n*-TiO_2. In contrast, significant mortalities occurred in *n*-TiO_2 treatments in the absence of food in dose-dependent manner ($p < 0.05$). Highest mortality occurred in 100 μg/mL suspensions. For 24-h exposure, values were 8.4, 5.3 and 6.3% for anatase, rutile and the mixture. Anatase appeared to be more toxic than rutile and mixture ($p < 0.05$). In 96 h, mortalities elevated to 29, 18 and 25% for anatase, rutile and the mixture, in that anatase polymorph was clearly the most toxic form ($p<0.05$). The mortality from mixture (25%) was also notably higher than that of rutile ($p<0.05$), which is likely due to high anatase composition (70%). Despite the elevated toxicity, none of the *n*-TiO_2 polymorphs were acutely toxic to artemia ($LC_{50} > 100$ μg/mL). These results are consistent with those reported previously (Zhu et al. 2010; Ates et al. 2013a). Dose- and time-dependent mortalities were also reported. While mortalities were negligible in 24 h, the same suspensions (1 μg/mL *n*-TiO_2) caused about 24% mortality on *D. magna* in 72 h (Zhu et al., 2010).

Presence of food in the exposure medium alleviated the mortalities. In 24 h, mortalities for rutile and mixture were not different from that of controls ($p>0.05$) and that for anatase was marginal ($p\geq0.05$). In 96 h, mortalities increased in a dose-dependent manner and were 16, 11 and 13% for anatase, rutile and mixture for the 100 μg/mL suspensions. These values were significantly lower than those observed without food ($p<0.05$), yet the order toxicity was the same; anatase was the most toxic and the rutile was the most benign form of *n*-TiO_2. *Artemia* are more resilient to toxic effects and food deprivation than daphnia (Zhu et al., 2010), and therefore, the short-term effects of exposure were readily tolerated. Yet, the results indicate significant suffering (e.g., mortality) under prolonged exposures which could be due to food deprivation. In a previous report, the mortalities from *n*-TiO_2 were also ascribed to starvation due to depletion of food supply within 96 h (Ates et al., 2013a).

Effects of *n*-TiO_2 crystal phase and food availability on oxidative stress in *Artemia salina*

Total malondialdehyde (MDA) concentrations measured as an indicator of lipid peroxidation are illustrated in Figure 7. The MDA levels were influenced from the availability of food ($p<0.05$). When food is present, no significant oxidative stress was noted in 24 h ($p > 0.05$). In contrast, both 10 and 100 μg/mL *n*-TiO_2 suspensions induced significant oxidative stress in 24 h in the absence of food ($p<0.05$). Average MDA concentration about 11.8 nmol/g in artemia exposed to 100 μg/mL anatase suspensions. This level was also statistically different than from those of rutile (7.7 nmol/g) and anatase/rutile mixture (8.9 nmol/g) pointing to the toxicity of anatase form.

Food deprivation elevates lipid peroxidation levels due to the increasing generation of oxygen free radicals as the antioxidant levels deplete as a result of starvation (Pascual et al., 2003). In this study, prolonged exposure (e.g., 96 h) resulted in higher oxidative stress on artemia. In the absence of food, mean MDA levels were as high as 25.0, 21.8 and 23.0 and nmol/g for at 100 μg/mL suspensions of anatase, rutile and anatase/rutile polymorphs, respectively. Feeding during the exposure greatly reduced the oxidative stress on artemia ($p < 0.05$). MDA levels for 100 μg/mL treatments were 17.2, 11.5 and 13.2 for anatase, rutile and anatase/rutile mixture polymorphs, respectively. Nonetheless, lethal effects occurred for all polymorphs among that anatase *n*-TiO_2 were more deleterious ($p < 0.05$). These results are consistent with the toxic effects reported for *n*-TiO_2 (Hsiao & Huang, 2011). Anatase polymorph was reported to induce higher oxidative stress on *E. coli* than mixture of anatase/rutile, where effects were ascribed to increased interaction of anatase polymorph with *E.coli* (Lin et al., 2014). Lethal effects associated with oxidative stress are influenced by the endurance of the species. *D. magna* suffered significant mortality due to oxidative stress (Kim et al., 2010) as occurred for artemia here, but marine abalone did survive under oxidative stress (Zhu et al., 2011).

CONCLUSIONS

Size and shapes of nanoparticles have long been known to mediate their toxic effects. In this study, anatase, rutile and anatase/rutile polymorphs of *n*-TiO_2 have been investigated in order to provide an understanding if differences in crystal phases would influence the nanoparticle's toxicity and other physico-chemical properties. The differences among crystal

phases of *n*-TiO_2 powders were evident following the characterizations by XRD, FTIR and SEM. The rutile was the most stable in water owing to high negative zeta potential (−31.6 mV), and consequently exhibited smaller size distribution and the lower agglomeration. Nonetheless, agglomeration was inevitable regardless of the crystal structure of *n*-TiO_2.

Free titanium levels measured from seawater were negligible for all crystal forms of *n*-TiO_2. Thus, it is concluded dissolution of *n*-TiO_2 is unlikely to induce any adverse effects on *Artemia salina*. In contrast, differences in *n*-TiO_2 polymorph phases were influential on accumulation. TiO_2 levels ingested increased in the order of rutile, anatase/rutile mixture and anatase. Because artemia unselectively filters particles from water, this effect was also thought to be related with the extent of particle agglomeration and elimination rates. In other words, greater accumulation of anatase was most likely due to inability of artemia to excrete relatively large of anatase aggregates from the guts. Food availability did substantially reduce the amount of accumulation either due to reduced feeding on TiO_2 particles or by facilitating the elimination of ingested particles from the guts. Differences in crystal structure were also found to affect the toxicity of *n*-TiO_2. The anatase polymorph constantly induced higher mortality and oxidative stress on artemia. These effects are corroborated with catalytic properties of anatase which is catalytically more active and stronger oxidizer than rutile; consequently induced higher lipid peroxidation. In conclusion, the results obtained for *n*-TiO_2 indicate that differences in crystalline phases of nanoparticles could influence their physicochemical status and toxicity in aquatic systems. *Artemia* is relatively more resilient to chemical toxicity and thus showed marginal suffering from *n*-TiO_2. It is expected that the extent of toxicity would vary with different species. Further, the results underlie the fact that observed effects from nanoparticles are highly complex combination of particle- and environment-related factors that necessitate continuing efforts for accurate understanding of safety issues of nanomaterials.

Acknowledgments

This project is funded in part by grants from the National Institutes of Health (NIH) through Research Centers in Minority Institutions (RCMI) Program at Jackson State University (Grant No: G12RR013459). The views expressed herein are those of authors and do not necessarily represent the official views of the funding agencies, and any of their sub-agencies.

References

Aruoja V, Dubourguier HC, Kasemets K, Kahru A. Toxicity of nanoparticles of CuO, ZnO and TiO_2 to microalgae *Pseudokirchneriella subcapitata*. Sci Tot Environ. 2009; 407:1461–1468.

Ates M, Daniels J, Arslan Z, Farah IO. Effects of aqueous suspensions of titanium dioxide nanoparticles on Artemia salina: assessment of nanoparticle aggregation, accumulation, and toxicity. Environ Monit Assess. 2013a; 185:3339–3348. [PubMed: 22810381]

Ates M, Daniels J, Arslan Z, Farah IO, Rivera HF. Comparative evaluation of impact of Zn and ZnO nanoparticles on brine shrimp (*Artemia salina*) larvae: effects of particle size and solubility on toxicity. Environ Sci: Processes & Impacts. 2013b; 15:225.

Battin TJ, Kammer FDD, Weilhartner A, Ottofuelling S, Hofmann T. Nanostructured TiO_2: Transport behavior and effects on aquatic microbial communities under environmental conditions. Environ Sci Technol. 2009; 43:8098–8104. [PubMed: 19924929]

Bundschuh M, Seitz F, Rosenfeldt RR, Ralf Schulz R. Titanium dioxide nanoparticles Increase sensitivity in the next generation of the water flea *Daphnia magna*. PLoS One. 2012; 7(11):e48956. [PubMed: 23145038]

DeMatteis V, Cascione M, Brunetti V, Toma CC, Rinaldi R. Toxicity assessment of anatase and rutile titanium dioxide nanoparticles: The role of degradation in different pH conditions and light exposure. Toxicol in Vitro. 2016; 37:201–210. [PubMed: 27622577]

El-Sherbiny S, Morsy F, Samir M, Fouad OA. Synthesis, characterization and application of TiO_2 nanopowders as special paper coating pigment. Appl Nanosci. 2014; 4:305–313.

Fanga Q, Shi X, Zhang L, Wang Q, Wang X, Guo Y, Zhou B. Effect of titanium dioxide nanoparticles on the bioavailability, metabolism, and toxicity of pentachlorophenolin zebrafish larvae. J Hazard Mater. 2015; 283:897–904. [PubMed: 25464334]

Handy RD, Henry TB, Scown TM, Johnston BD, Tyler CR. Manufactured nanoparticles: their uptake and effects on fish-a mechanistic analysis. Ecotoxicology. 2008; 17:396–409. [PubMed: 18408995]

Heinlaan M, Ivask A, Blinova I, Dubourguier HC, Kahru A. Toxicity of nanosized and bulk ZnO, CuO and TiO_2 to bacteria *Vibrio fischeri* and crustaceans *Daphnia magna* and *Thamnocephalus platyurus*. Chemosphere. 2008; 71:1308–1316. [PubMed: 18194809]

Hsiao IL, Huang YJ. Effects of various physicochemical characteristics on the toxicities of ZnO and TiO_2 nanoparticles toward human lung epithelial cells. Sci Tot Environ. 2011; 409:1219–1228.

Hu X, Cook S, Wang P, Hwang HM. In vitro evaluation of cytotoxicity of engineered metal oxide nanoparticles. Sci Tot Environ. 2009; 407:3070–3072.

Huang YW, Wu CH, Aronstam RS. Toxicity of transition metal oxide nanoparticles: recent insights from in vitro studies. Materials. 2010; 3:4842–4859. [PubMed: 28883356]

Hussain AA, Wahab HS. Synthesis and spectroscopic characterization of anatase TiO_2 nanoparticles. Int J Nanotechnology Nanosci. 2014; 2:1–6.

Jovanovi B. Review of titanium dioxide nanoparticle phototoxicity: developing a phototoxicity ratio to correct the endpoint values of toxicity tests. Environ Toxicol Chem. 2015; 34(5):1070–1077. [PubMed: 25640001]

Kadam AN, Dhabbe RS, Kokate MR, Gaikwad YB, Garadkar KM. Preparation of N doped TiO_2 via microwave-assisted method and its photocatalytic activity for degradation of Malathion. Spectrochim Acta A: Mol Biomol Spectrosc. 2014; 133:669–676. [PubMed: 24996208]

Kim KT, Klaine SJ, Cho JW, Kim SH, Kim SD. Oxidative stress responses of *Daphnia magna* exposed to TiO_2 nanoparticles according to size fraction. Sci Tot Environ. 2010; 408:2268–2272.

Klein SM, Choi JH, Pine DJ, Lange FF. Synthesis of rutile titania powders: Agglomeration, dissolution, and reprecipitation phenomena. J Mater Res. 2003; 18:1457–1464.

Lai JCK, Lai MB, Jandhyam S, Dukhande VV, Bhushan A, Daniels CK, Leung SW. Exposure to titanium dioxide and other metallic oxide nanoparticles induces cytotoxicity on human neural cells and fibroblasts. Int J Nanomedicine. 2008; 3:533–545. [PubMed: 19337421]

Lin X, Li J, Ma S, Liu G, Yang K, Tong M, Lin D. Toxicity of TiO_2 Nanoparticles to *Escherichia coli*: Effects of particle size, crystal phase and water chemistry. PLoS One. 2014; 9(10):e110247. [PubMed: 25310452]

Liu L, Zhao H, Andino JM, Li Y. Photocatalytic CO_2 reduction with H_2O on TiO_2 nanocrystals: Comparison of anatase, rutile, and brookite polymorphs and exploration of surface chemistry. ACS Catal. 2012; 2:1817–1828.

Lovern SB, Klaper R. *Daphnia magna* mortality when exposed to titanium dioxide and fullerene (C60) nanoparticles. Environ Toxicol Chem. 2006; 25:1132–1137. [PubMed: 16629153]

Luttrell T, Halpegamage S, Tao J, Kramer A, Sutter E, Batzill M. Why is anatase a better photocatalyst than rutile?- Model studies on epitaxial TiO_2 films. Sci Rep. 2014; 4:4043.doi: 10.1038/srep04043 [PubMed: 24509651]

Mansfield CM, Alloy MM, Hamilton J, Verbeck GF, Newton K, Klaine SJ, Roberts AP. Photo-induced toxicity of titanium dioxide nanoparticles to *Daphnia magna* under natural sunlight. Chemosphere. 2015; 120:206–210. [PubMed: 25062026]

Nolan N, Pillai S, Seery M. Spectroscopic investigation of the anatase-to-rutile transformation of sol-gel synthesized TiO_2 photocatalysts. J Phys Chem C. 2009; 113:16151–16157.

Nowack B, Bucheli TD. Occurrence, behavior and effects of nanoparticles in the environment. Environ Pollut. 2007; 150:5–22. [PubMed: 17658673]

OECD. Organisation for Economic Co-operation and Development (OECD). Guideline for the Testing of Chemicals (Part 202). 2004.

Pascual P, Pedrajas JR, Toribio F, Lopez-Barea J, Peinado J. Effect of food deprivation on oxidative stress biomarkers in fish (*Sparus aurata*). Chem-Biol Interact. 2003; 145:191–199. [PubMed: 12686495]

Paterson G, Ataria JM, Hoque ME, Burns DC, Metcalfe CD. The toxicity of titanium dioxide nanopowder to early life stages of the Japanese medaka (Oryzias latipes). Chemosphere. 2011; 82:1002–1009. [PubMed: 21074241]

Scown TM, Van Aerle R, Tyler CR. Review: Do engineered nanoparticles pose a significant threat to the aquatic environment? Crit Rev Toxicol. 2010; 40:653–670. [PubMed: 20662713]

Shirke BS, Korake PV, Hankare PP, Bamane SR, Garadkar KM. Synthesis and characterization of pure anatase TiO_2 nanoparticles. J Mater Sci: Mater Electron. 2011; 22:821–824.

Van der Vliet V, Tuinstra TJ, Rademaker B, Bast A. Intestinal motility disorder induced by peroxides: possible role of lipid peroxidation. Res Commun Chem Pathol Pharmacol. 1990; 70:227–43. [PubMed: 1980544]

Vijayalakshmi R, Rajendran V. Synthesis and characterization of nano-TiO_2 via different methods. Arch Appl Sci Res. 2012; 4:1183–1190.

Weir A, Westerhoff P, Fabricius L, Hristovski K, von Goetz N. Titanium dioxide nanoparticles in food and personal care products. Environ Sci Technol. 2012; 46:2242–2250. [PubMed: 22260395]

Zhu X, Chang Y, Chen Y. Toxicity and bioaccumulation of TiO_2 nanoparticles aggregates in *Daphnia magna*. Chemosphere. 2010; 78:209–215. [PubMed: 19963236]

Zhu X, Jin Z, Cai Z. The toxicity and oxidative stress of TiO_2 nanoparticles in marine abalone (*Haliotis diversicolor supertexta*). Mar Pollut Bull. 2011; 63:334–338. [PubMed: 21492882]

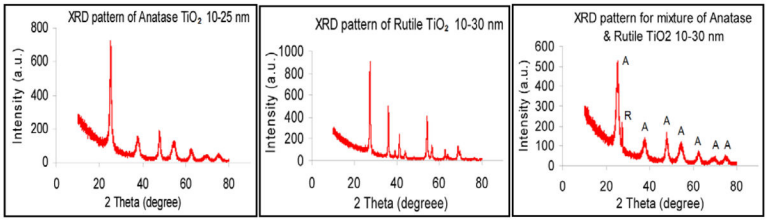

Figure 1.
X-ray diffraction (XRD) patterns of anatase, rutile, and anatase/rutile mixture *n*-TiO_2.

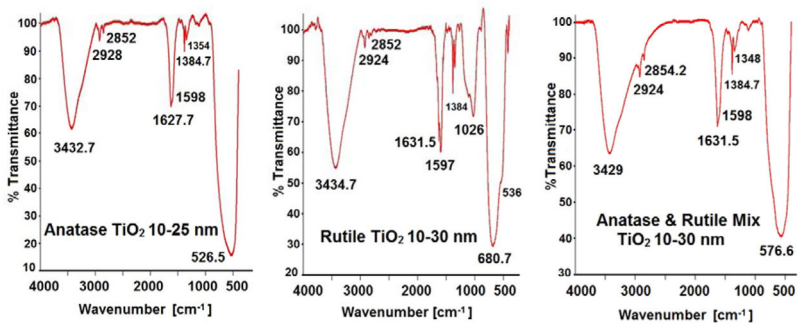

Figure 2.

Infrared spectra for anatase, rutile, and anatase/rutile mixture of *n*-TiO_2.

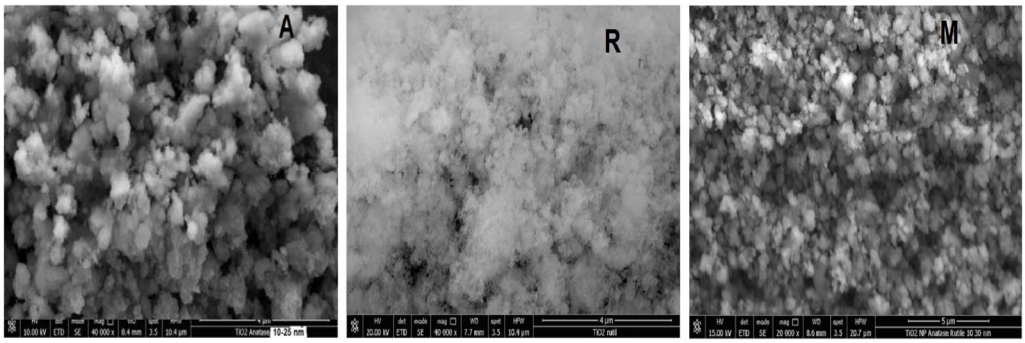

Figure 3.
SEM images of *n*-TiO_2 powders. (A) anatase, (B) rutile and (M) mixture.

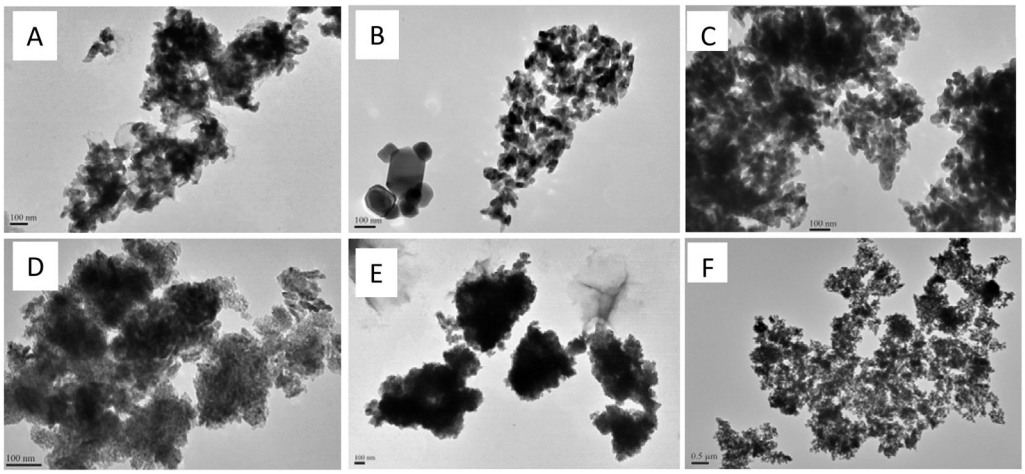

Figure 4.

TEM images of different polymorphs of *n*-TiO_2. (A) Anatase, (B) Rutile and (C) anatase/rutile mixture in deionized water. (D) Rutile, (E) Anatase, and (F) anatase/rutile mixture in seawater. Images were acquired from 10 μg/mL aqueous colloids.

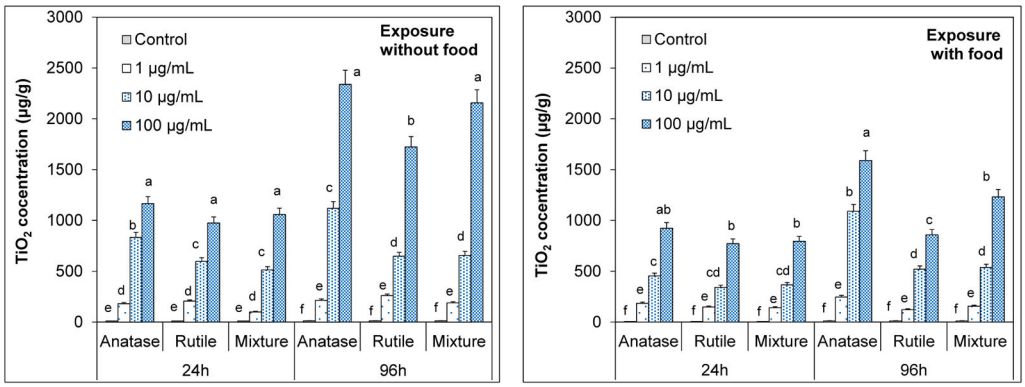

Figure 5.

Accumulation patterns of anatase, rutile and anatase/rutile mixture polymorphs of *n*-TiO_2 by *Artemia salina* larvae across a concentration gradient in the presence and absence of food in 24h and 96h. The values are mean ± standard deviation for three replicate measurements (n=3). Values denoted with different letters within same exposure period are statistically different ($p < 0.05$).

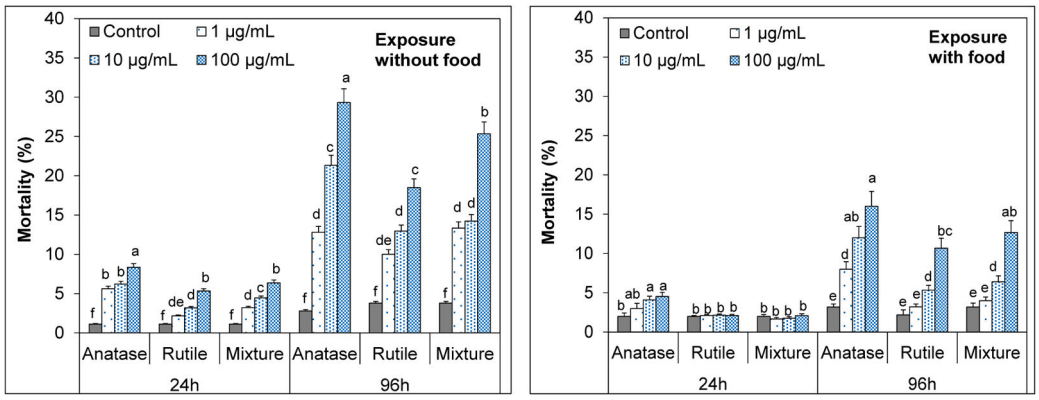

Figure 6.

Percent mortalities for *Artemia salina* larvae measured in suspensions of anatase, rutile and anatase/rutile mixture polymorphs of *n*-TiO_2 in the presence and absence of food in 24h and 96h. The values are mean ± standard deviation for three replicate measurements (n=3). Values denoted with different letters within same exposure period are statistically different ($p < 0.05$).

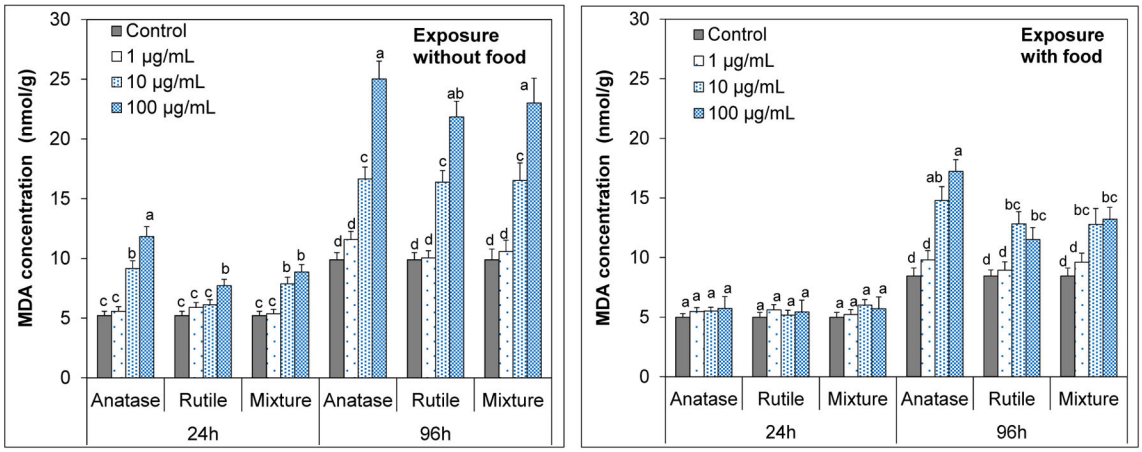

Figure 7.

Malondialdehyde (MDA) levels (nmol/g) in exposed *Artemia salina* larvae after 24h and 96h exposure to anatase, rutile and anatase/rutile mixture polymorphs of *n*-TiO_2 in the presence and absence. The values are mean ± standard deviation for three replicate measurements (n=3). Values denoted with different letters within same exposure period are statistically different ($p < 0.05$).

Table 1

Some physical properties of the TiO_2 nanopowders investigated in this study

***n*-TiO_2 polymorph**	**Size (nm, D_{50})**	**Surface area (m^2/g)**	**Color**
Anatase (99.5%)	10–25	50–150	White
Rutile (99.5%)	10–30	50	Pale Yellow
Mixture (30% rutile, 70% anatase)	10–30	50–100	White

Table 2

Experimental conditions for acute exposure of *Artemia salina* larvae to different polymorphs of *n*-TiO_2

Regime	*n*-TiO_2 (μg/mL)	pH	N° of *Artemia salina* larvae (x10^3)					
			Exposure with food			Exposure without food		
			Anatase	Rutile	Mixture	Anatase	Rutile	Mixture
24 h	0	8.2 – 8.6	15.8	15.8	15.8	19.3	19.3	19.3
	1	8.1 – 8.4	14.6	19.7	18.6	16.2	15.2	21.2
	10	8.2 – 8.4	20.2	11.6	18.4	18.5	13.9	16.2
	100	8.1 – 8.6	19.4	18.4	19.7	16.8	18.3	14.5
96 h	0	8.3 – 8.6	22.3	22.3	22.3	14.8	14.8	14.8
	1	8.3 – 8.8	20.7	16.5	22.9	21.3	18.7	12.3
	10	8.2 – 8.6	21.5	20.9	21.5	19.8	20.7	15.6
	100	8.4 – 8.7	20.1	16.4	16.9	22.4	17.5	14.9

Table 3

Hydrodynamic sizes and zeta potentials of anatase, rutile and anatase/rutile mixture of *n*-TiO_2 in water

***n*-TiO_2 polymorph**	**Size range(nm)**	**Z-Average(nm)**	**Zeta potential(mV)**
Anatase	265 – 1335	637	−16.7 ± 4.2
Rutile	61 – 1152	432	−31.6 ± 4.5
Mixture	356 – 859	662	−15.7 ± 4.9

Z-averages are calculated by the Zeta sizer software. The data for three replicate measurements.

Table 4

Dissolved titanium concentration (ng/mL) measured from the suspensions of *n*-TiO_2 in seawater suspensions. Values are given as average ± standard deviation of three separate analyses

***n*-TiO_2 concentration**	**Anatase**		**Rutile**		**Mixture**	
	24 h	**96 h**	**24 h**	**96 h**	**24 h**	**96 h**
1 μg/mL	46.0 ± 3.9	82.7 ±4.3	40.9 ± 2.0	86.4 ± 5.9	42.1 ± 5.0	84.6 ±5.9
10 μg/mL	65.9 ± 3.9	88.1 ± 5.4	57.2 ± 3.9	87.5 ± 3.0	54.6 ± 5.4	91.7 ± 6.4
100 μg/mL	78.8 ± 5.8	95.7 ± 4.9	85.8 ± 4.3	97.1 ± 5.8	71.3 ± 5.8	119 ± 8.1